The Astrophysical Journal, 889:97 (10pp), 2020 February 1 https://doi.org/10.3847/1538-4357/ab643c
© 2020. The American Astronomical Society. All rights reserved.

The Original Anisotropy of TeV Cosmic Rays in the Local Interstellar Medium

Ming Zhang[1], N. V. Pogorelov[2], Y. Zhang[3], H. B. Hu[3,4], and R. Schlickeiser[5]
[1] Department of Physics and Space Sciences, Florida Institute of Technology, 150 W. University Boulevard, Melbourne, FL 32901, USA; mzhang@fit.edu
[2] Department of Space Science and Center for Space Plasma and Aeronomic Research, University of Alabama in Huntsville, 320 Sparkman Drive, Huntsville, AL 35899, USA
[3] Key Laboratory of Particle Astrophysics, Institute of High Energy Physics, Chinese Academy of Sciences, Beijing 100049, People's Republic of China
[4] The University of Chinese Academy of Sciences, 19A Yuquan Road, Beijing 100049, People's Republic of China
[5] Institut für Theoretische Physik, Lehrstuhl IV: Weltraum- und Astrophysik, Ruhr-Universität Bochum, D-44780 Bochum, Germany
Received 2019 September 25; revised 2019 December 16; accepted 2019 December 18; published 2020 January 29

Abstract

This paper presents the original anisotropy that TeV cosmic rays (CRs) have in the local interstellar medium. This anisotropy is obtained using a method of flux mapping with the Liouville theorem and a magnetohydrodynamic (MHD) heliosphere model of the electromagnetic field to remove the particle propagation effects hidden in the measurements made by the Tibet ASγ experiment at Earth. The original interstellar anisotropy turns out to be almost a pure dipole, which results from a diffusion flow of CRs escaping along the local interstellar magnetic field into the northern Galactic halo. The observed anisotropy maps at Earth appear quite complex because the heliosphere distorts the dipole anisotropy, generating a significant amount of high-order multipoles, while interstellar magnetic field fluctuations contribute to some weak anisotropy on small angular scales. It is found that the density gradient of these CRs points approximately toward Vela in the Local Bubble, providing experimental evidence to show that the local supernova is making a special contribution to the TeV CRs we see at Earth. This special contribution will keep growing in the future tens of thousand years. The original anisotropy also reveals that the CRs spread from the source primarily along the interstellar magnetic field, while experiencing a nearly isotropic pitch-angle scattering process caused by interstellar turbulence.

Unified Astronomy Thesaurus concepts: Heliosphere (711); Galactic cosmic rays (567); Cosmic ray sources (328)

1. Introduction

Although almost all theories suggested that Galactic cosmic rays (CRs) below the knee energy (~3000 TeV) are accelerated by supernova shocks, so far no experimental evidence has been obtained for any individual supernova making a particular contribution to the CRs we see at Earth. Anisotropy measurements can be used to search for an excess of CRs from a particular object in the sky. Vela, approximately 815 lt-yr away, is the closest known supernova remnant. However, the gyroradii of CRs below the knee energy in the typical interstellar magnetic field are less than 1 lt-yr. Their mean free path due to scattering on turbulent fluctuations is roughly a few light years. CRs must have lost most of the directional information about their sources. Furthermore, CRs may come from many sources, thus mixing their directional information together in random fashions. Indeed, observations show that the anisotropy of TeV CRs is rather small, about 10^{-4}–10^{-3} in relative intensity (e.g., Amenomori et al. 2006; Abbasi et al. 2011; Abeysekara et al. 2019). Several experiments have accumulated enough measurements to construct two-dimensional anisotropy sky maps in their respective fields of view. Figure 1(A) shows an example of partial-sky map obtained by the Tibet ASγ experiment (Amenomori et al. 2006). Recently, experiments in the northern and southern hemispheres combined their data to produce nearly full-sky maps (Abeysekara et al. 2019). The observed anisotropy patterns appear quite complex and puzzling, making hard to interpret with the traditional diffusion-convection theory of CR transport.

The interstellar transport of CRs is governed by several processes: convection, drift in magnetic fields, diffusion driven by turbulence, and energy changes due to electric fields. Each of these causes anisotropy. These effects mix together in observed maps. In a uniform large-scale magnetic field with small fluctuations, the diffusion and drift anisotropies are mainly dipolar. The Compton–Getting anisotropy (Compton & Getting 1935) due to the Sun's motion with respect to the local interstellar medium (LISM) plasma/gas is also dipolar. Thus, we expect to see a dipolar anisotropy as a sum of dipoles is still a dipole. Particle mirroring by inhomogeneities in the LISM magnetic field (LISMF) may contribute additional quadrupole anisotropy. However, the observed pattern (see Figure 1(A)) is not that simple. By decomposing the anisotropy into a series of spherical harmonics, the IceCube team found that there is a significant amount of spectral power in high-order multipoles (Abbasi et al. 2011), suggesting that CR anisotropy exhibits structures on intermediate and small angular scales. The observations seem to disagree with the traditional theory of CR transport. The origin of TeV CR anisotropies remains a puzzle after a decade of active research and numerous proposed explanations. It was suggested that small-scale enhancements in the CR intensity might arrive from certain specific point sources in the Galaxy (Amenomori et al. 2006; Abbasi et al. 2011). Some researchers argue that LISM turbulence might produce small-scale anisotropy (Giacinti & Sigl 2012; Ahlers & Mertsch 2015). The Tibet team noticed that some anisotropy features in their observations are aligned with the so-called hydrogen deflection plane (HDP), the plane containing the original LISM (neutral helium) flow vector and the flow vector of deflected neutral hydrogen caused by the solar wind (SW)–LISM interaction (Amenomori & The Tibet ASγ Collaboration 2010). This provides the first evidence for the heliospheric modulation of TeV CRs. Subsequently, theories and models have been proposed to explain how the heliosphere can affect the anisotropy (Desiati & Lazarian 2013; O'C. Drury 2013; Schwadron et al. 2014; Zhang et al. 2014).

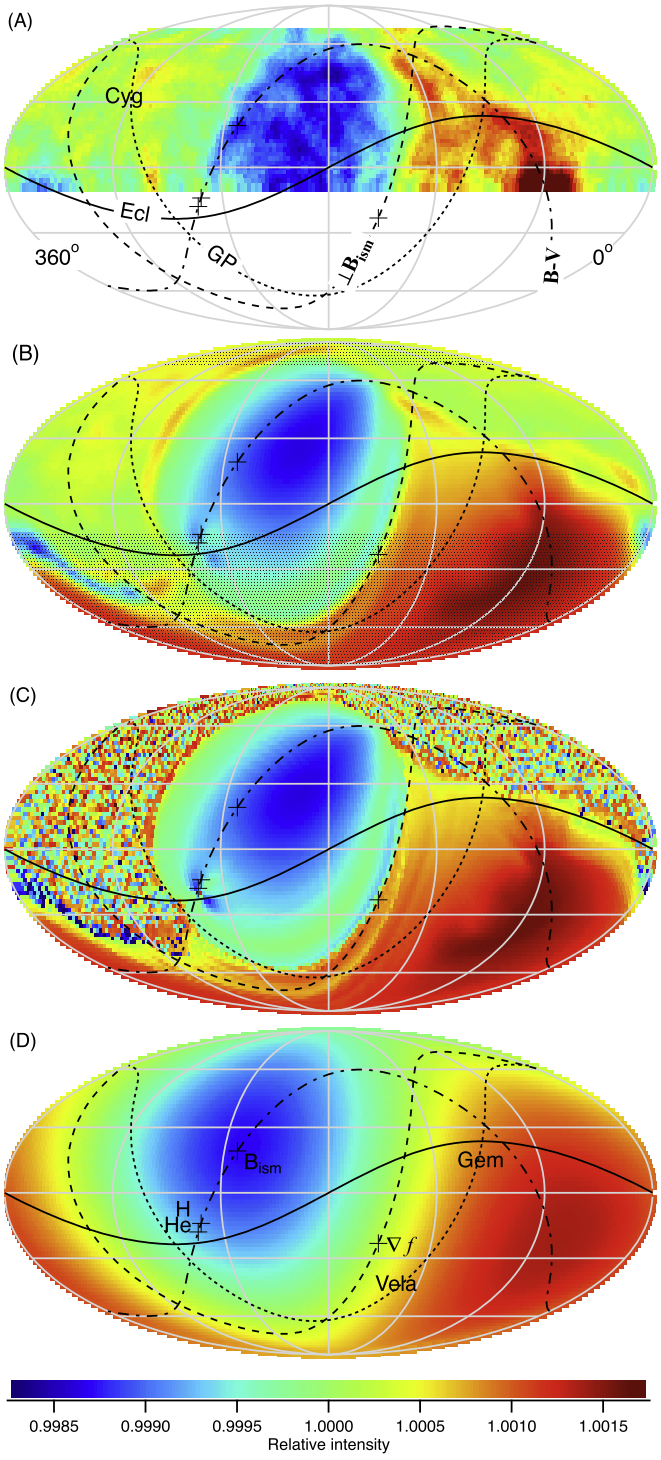

Figure 1. Anisotropy maps of 4 TeV CR relative intensity in the celestial coordinate system. (A) Tiber ASγ measurements at Earth sampled at $2^\circ \times 2^\circ$ resolution and averaged over 5° radius (Amenomori et al. 2006). (B) Model calculation of anisotropy expected at Earth after the distortion by the heliosphere in 5° averages with light shading outside of the Tibet ASγ field of view. (C) Model calculation of anisotropy after the heliospheric distortion without average. (D) Inferred large-scale anisotropy in the pristine LISM if the heliosphere is not present. The curves represent the locations of the ecliptic (ECL), Galactic (GP), Hydrogen deflection ($B-V$) and LISMF equator ($\perp \boldsymbol{B}_{\rm ism}$) planes. The crosses indicate the directions of LISM helium inflow (He), LISM hydrogen inflow (H), LISMF ($\boldsymbol{B}_{\rm ism}$) and CR density gradient (∇f).

Earth resides deep in the heliosphere. The trajectories of CRs measured in experiments are affected by the electromagnetic fields of the heliosphere and disturbed LISM surrounding it. This may severely distort the anisotropy maps. To study the properties of interstellar CRs, we must first remove the heliospheric influence. Recent advances in the heliospheric physics and modeling based on observations from *Voyager* and the *Interstellar Boundary Explorer* (*IBEX*) have made this task possible. In this paper, we reconstruct the anisotropy of TeV CRs in the pristine LISM. The results reveal a potential source of CR anisotropy and shed light onto the eternal question about the origin of CRs and their transport mechanisms through the ISM to reach Earth.

2. Method

2.1. Liouville Mapping

The intensity of CRs at a fixed energy is proportional to the particle distribution function or phase-space density in the reference frame of the observer. CR anisotropy as a distribution function of momentum vector $\boldsymbol{p}_{\rm o}$ observed at Earth $\boldsymbol{x}_{\rm o}$, $f(\boldsymbol{x}_{\rm o}, \boldsymbol{p}_{\rm o})$, can be mapped from the particle distribution function in the LISM plasma frame $f(\boldsymbol{x}, \boldsymbol{p})$ with the help of the Liouville theorem, which states that the distribution function is invariant along any particle trajectory and for any transformation of the reference frame (Bradt & Olbert 2008). The Liouville theorem is valid as long as all the forces acting the particles along the trajectories are known. The electromagnetic fields in the heliosphere and surrounding LISM are calculated with our MHD heliosphere model. Unknown fluctuating fields are neglected because the scattering time of TeV CRs is much longer than the propagation time during the passage of the heliosphere. Once the electromagnetic field is found, CR trajectories can be calculated using the Lorentz force, so that we can map momentum $\boldsymbol{p}_{\rm o}$ at Earth to momentum $\boldsymbol{p}$ in the LISM. Such mappings can cause complex shifts in the anisotropy pattern.

As the amplitude of observed anisotropy of TeV CRs is small in the order of 10^{-3} (Amenomori et al. 2006), for the purpose of modeling large-scale anisotropy, it is logical to assume that the distribution function of CRs of charge q as a function of position $\boldsymbol{x}$ and momentum $\boldsymbol{p}$ in the LISMF $\boldsymbol{B}_{\rm ism}$ is weakly dependent on particle guiding center $\boldsymbol{R} = \boldsymbol{x} + \boldsymbol{p} \times \boldsymbol{B}_{\rm ism}/(qB_{\rm ism}^2)$ and pitch-angle cosine $\mu = \boldsymbol{p} \cdot \boldsymbol{B}_{\rm ism}/(pB_{\rm ism})$, so that it can be expressed in the following perturbation form:

$$f(\boldsymbol{x}_{\rm o}, \boldsymbol{p}_{\rm o}) = f(\boldsymbol{x}, \boldsymbol{p}) = f_0[1 + A_1 P_1(\mu) + A_2 P_2(\mu) + \boldsymbol{G}_\perp \cdot \boldsymbol{R}](p/p_{\rm o})^{-(2+\gamma)}, \quad (1)$$

where $\boldsymbol{G}_\perp = \nabla_\perp \ln f$ is the CR density gradient vector perpendicular to the LISMF, A_1 and A_2, are the amplitude associated with the first and second-order Legendre polynomials, $P_1(\mu)$ and $P_2(\mu)$, respectively. The parameter γ is the CR spectral slope, approximately equal to 2.75 according to measurements of CR spectrum. A detailed description of the Liouville mapping method and its implications to the mechanisms producing CR anisotropies can be found in Zhang et al. (2014). Note that with Equation (1), higher-order anisotropies (beyond the quadrupole) in the LISM are considered as unmodeled residues.

To determine the parameters specifying the gradient and pitch-angle anisotropy, we use the standard least-weighted χ^2 method to fit the anisotropy calculation using Equation (1) to the measurements of relative intensity $I(\boldsymbol{p}_{{\rm o}m})$ with its statistical error bar $\sigma(\boldsymbol{p}_{{\rm o}m})$ for each pixel m obtained by Tibet ASγ

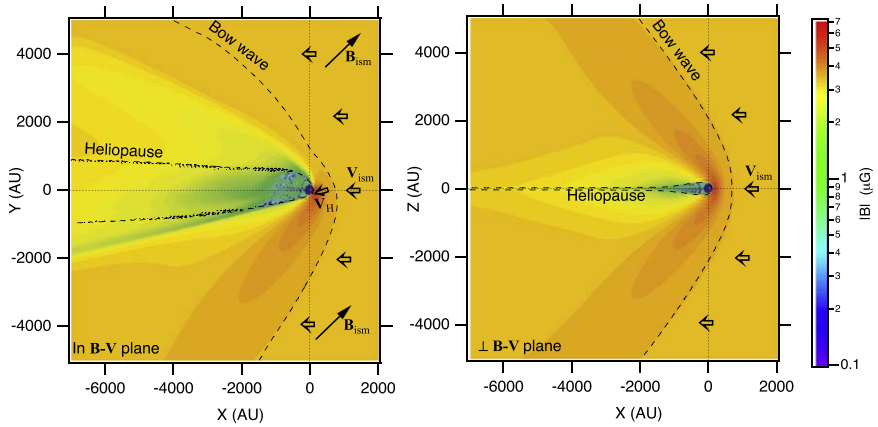

Figure 2. Distribution of magnetic field strength in the $B-V$ plane (left) and the plane perpendicular to the $B-V$ plane (right). The dashed lines indicate the locations of the heliopause and heliospheric bow wave. It is the deviation of the magnetic field and plasma flow from their LISM quantities that distorts the picture of CR anisotropy. Arrows show the direction of the LISMF ($\boldsymbol{B}_{\rm ism}$), LISM flow ($\boldsymbol{V}_{\rm ism}$) and deflected flow of neutral hydrogen entering the heliophere ($\boldsymbol{V}_{\rm H}$).

experiment (Amenomori et al. 2006):

$$\chi^2 = \sum_{m=1}^{M}\left[\frac{I(\boldsymbol{p}_{\rm om}) - f(\boldsymbol{x}_m, \boldsymbol{p}_m)}{\sigma(\boldsymbol{p}_{\rm om})}\right]^2. \quad (2)$$

Tibet ASγ experiment is located at Yangbajing (90°.522 E, 30°.102 N; 4300 m above sea level) in Tibet, China (Amenomori et al. 2006). The experiment covers a partial sky, roughly from $\sim -10°$ to 68° in decl., as shown in Figure 1(A). The experimental results of relative intensity and its significance maps have been published previously, so the details of measurements and data processing are not given here. The overall pattern of CR anisotropy does not change between 3 and ~20 TeV, so we choose 4 TeV measurements for detail modeling. IceCube-HAWC experiments have recently published a combined CR anisotropy sky map of a larger field of view at 10 TeV (Abeysekara et al. 2019). However, we have not been able to obtain the data. The anisotropy pattern in the combined map looks similar to the Tibet ASγ result at 4 TeV within the common field of view, so we expect that future inclusion of the combined map will slightly improve our analysis. As the measured relative intensity $I(\boldsymbol{p}_{oi})$ is normalized to 1 over the instrument field of view, but the mapping between particle momentum $\boldsymbol{p}_{\rm o}$ at Earth $\boldsymbol{x}_{\rm o}$ and $\boldsymbol{p}$ at a location in the LISM $\boldsymbol{x}$ covers a different field of view, the normalization constant f_0 can deviate slightly from 1. As a result, f_0 becomes an additional free parameter for fitting the measurements. One could further make a Taylor expansion of f_0 around 1 to linearize Equation (1) in term of the fitting parameters, but it is necessary with a nonlinear-fitting algorithm. The method of χ^2 minimization to find best fitting parameters and their error bars are described in typical textbook (e.g., Taylor 1997, Chapter 8).

2.2. Heliosphere Model

To map the distribution function to Earth $f(\boldsymbol{x}_{\rm o}, \boldsymbol{p}_{\rm o})$ from the LISM $f(\boldsymbol{x}, \boldsymbol{p})$, CR trajectories are calculated using the Lorentz force exerted by the electromagnetic field obtained from our MHD heliospheric simulations (Pogorelov et al. 2015, 2017). The Sun heats and accelerates its coronal plasma to create a magnetized SW. The SW carves a bubble in the LISM, known as the heliosphere. The heliosphere is bounded by a surface called the heliopause, which prevents the LISM plasma and magnetic field from mixing with the SW. Before the SW reaches the heliopause, a termination shock forms to slow it down. Both the termination shock and the heliopause have been examined by the *Voyager 1* and *2* spacecraft with in situ observations of magnetic field and particles. The heliosphere moves through the LISM supersonically. However, the magnetization and charge exchange processes in the LISM make it uncertain whether a bow shock or a smooth bow wave forms in front of the heliosphere. The lack of in situ observations of the heliospheric bow wave does not allow us to know how far exactly it expands. Figure 2 illustrates the magnetic field structure of the SW–LISM interaction regions obtained in our simulations with the Multi-Scale Fluid-Kinetic Simulation Suite (MS-FLUKSS). It solves the ideal MHD equations with the source terms due to charge exchange between ions and neutral atoms, gravity, photoionization, nonthermal ions, and turbulence. The SW and heliospheric magnetic field parameters are built upon in situ measurements of the interplanetary medium by an array of heliospheric space missions. The LISM parameters are indirectly constrained to fit several observational data sets (Pogorelov et al. 2017). For example, they are used to explain in situ measurements of the termination shock, heliopause, plasma, magnetic field, and energetic particles from *Voyager* and *IBEX* observations of energetic neutral atoms (e.g., Zirnstein et al. 2016), and *Solar and Heliospheric Observatory* (*SOHO*) Lyα back-scattered emission (Pogorelov et al. 2017). MS-FLUKSS is highly parallelized and uses an adaptive mesh refinement technique to improve the accuracy of simulations. In this study, we also take into account the solar cycle effects to avoid the accumulation of solar magnetic field anywhere inside the heliosphere (Pogorelov et al. 2015). The boundary conditions of the unperturbed LISM parameters are only partially constrained by observations (Zirnstein et al. 2016), we further use TeV CR anisotropy measurements to confirm or refine them. This is mainly because the particle density and LISMF measured by *Voyager* and *IBEX* slightly outside of the heliopause have already been somewhat modified by the presence of the heliosphere.

The bow wave can extend to a heliocentric distance of 800 au in the upstream direction. It takes a few hundred years for the partially ionized ISM gas to cross it. Deceleration of the

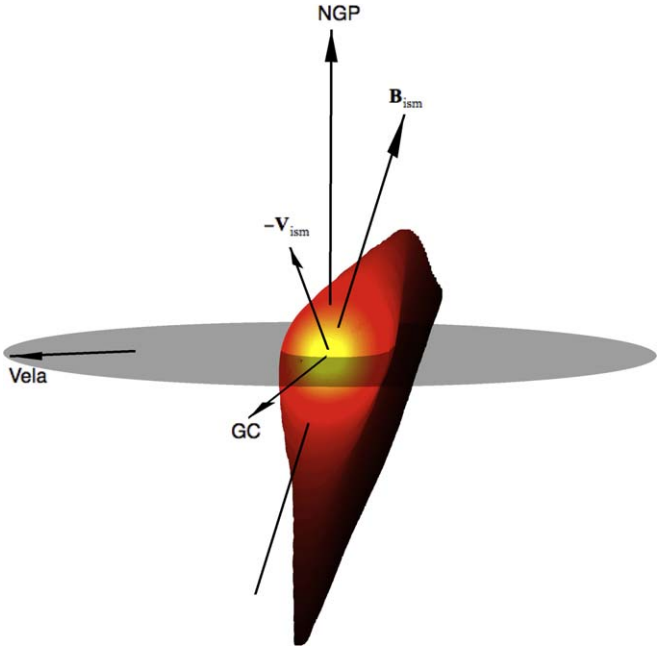

Figure 3. Three-dimensional plot of the heliopause surface to show its orientation in a Galactic coordinate system. It is viewed from a direction slightly off the nose of the heliosphere and above the Galactic plane. The tail beyond 2500 au downstream has been truncated. The heliopause is illuminated from the front of the nose with a bright gold color. The tail becomes darker with increasing distance from the Sun. The gray disk is the plane parallel to the Galactic plane. The arrows indicate the direction of the North Galactic pole (NGP), Galactic center (GC), LISMF ($\boldsymbol{B}_{\rm ism}$), the inflow of LISM relative to the Sun ($-\boldsymbol{V}_{\rm ism}$), and Vela supernova remnant (Vela).

LISM plasma by the heliopause results in an enhanced charge exchange in this region, and forms a so-called hydrogen wall. Charge exchange creates a heliospheric boundary layer of depressed plasma density in front of the heliopause. The heliospheric boundary does not allow all neutral hydrogen to enter the heliosphere freely. As a result, its bulk or average velocity direction in the heliosphere is different from its original direction in the unperturbed LISM. It has been shown in simulations (Pogorelov et al. 2009) that the HDP closely follows the $B-V$ plane, the plane containing both the LISMF and flow velocity vectors.

Voyager and *IBEX* observations can only partially constrain the determination of the unperturbed LISMF and ion density. We have run more than a dozen heliosphere models with LISMF strength ranging from 2.5 to 4.5 μG under the constraint set by *IBEX* and *Voyager* (Zirnstein et al. 2016; Pogorelov et al. 2017). The direction of the LISMF is constrained in the HDP up to 30° away from the center of *IBEX* ribbon, while the LISMF strength and ion density co-vary according to Zirnstein et al. (2016). Our best fits to the CR anisotropy observations impose new constraints on the LISMF, and neutral atom and ion densities used in our MHD model. The heliosphere configuration shown in Figures 2 and 3 is calculated with the LISMF strength of 3.5 μG, plasma density 0.065 $\rm cm^{-3}$, and neutral atom density 0.184 $\rm cm^{-3}$. The direction of LISMF (R.A. 232.°5 and decl. 19.°0 is indicated by the $\boldsymbol{B}_{\rm ism}$ symbol in Figures 1–5. It situates in the HDP, ∼5° away from the center of *IBEX* ribbon and ∼38° away from the helionose. On the Galactic coordinates, it is inclined to the Galactic disk by 53° and points northward as shown in Figure 3. This model allows us to best reproduce the TeV CR anisotropy observations with the smallest χ^2. The results give us confidence in the global-scale accuracy of our model and model parameters even though our model contains the sophisticated physics of the SW–LISM interaction and complicated mapping pattern of CR momentum from the LISM to Earth.

Because of the LISMF draping, the heliosphere is highly compressed in the direction perpendicular to the $B-V$ plane. As shown in Figure 2, the heliopause has the largest flaring in the $B-V$ plane. Due to the pressure the LISMF exerts on the surface of the heliopause, the latter is more compressed in directions perpendicular to the $B-V$ plane. The heliopause gets thinner further downstream as the hot heliotail protons are substituted by colder protons born of the LISM neutral atoms in the process of charge exchange. Figure 3 shows a 3d picture of the heliopause surface in the Galactic coordinates. It gives us a near-frontal view of the heliopause, while the heliotail is truncated at 2500 au. The magnetic field in the surrounding LISM at distances exceeding 10,000 au is still affected by the presence of the heliopause. It is the deviation of the magnetic field inside the bow wave from the original LISMF that mainly makes TeV CRs reach Earth on trajectories different from their original helical paths and thus cause distortion of anisotropy when we observe inside the heliosphere. Due to the large gyroradii of TeV CRs, our model covers the heliotail to distances up to 10,000 au to account for all the heliospheric disturbances made to TeV CR trajectories. In most regions inside the heliopause, the heliospheric magnetic field of the solar origin is much weaker than and occupies much smaller volume than the LISMF outside of the heliopause, and TeV CR trajectories are nearly straight lines. The exact field polarity, phase of the solar cycle, strength, and fluctuation of the heliospheric magnetic field of the solar origin is not important, which results in weak variations of the TeV CR anisotropy over the solar cycle (Amenomori et al. 2006; Zhang et al. 2014).

3. Result

3.1. Reproduction of Anisotropy Sky Map Observed on Earth

Figures 1(B) and (C) show the results of our calculations of anisotropy for 4 TeV CRs after the least χ^2 fit to the observation is performed to fix the parameters in the LISM CR distribution function. Table 1 lists the derived values of these parameters. The calculated CR anisotropy in Figure 1(C) is sampled every 2° in both decl. and R.A. There is a substantial part of the sky in the map that displays rapid, large fluctuations of CR intensity, indicating that the heliosphere and its surrounding LISM are almost completely translucent for us to see the background LISM CR anisotropy. These large fluctuations are due to chaotic motion of CRs through the medium downstream of the Sun. They are sensitive to arrival directions, as well as to small fluctuations in the heliospheric magnetic field. The enhancement of CR intensity in the direction of Cygnus Constellation reported by the Tibet ASγ team (Amenomori et al. 2006) is actually located in this part of the sky. The enhancement of CR intensity in the Cygnus region could be due to coincidental heliospheric fluctuations. It is consistent with (McComas et al. 2010), who show that some heliospheric structures in this region seen in *IBEX* neutral atoms images are time-variable.

The measurements shown in Figure 1(A) are averages over circles of 5°-radius from the center of each pixel. Correspondingly, our calculations are also averaged over multiple (>250 random)

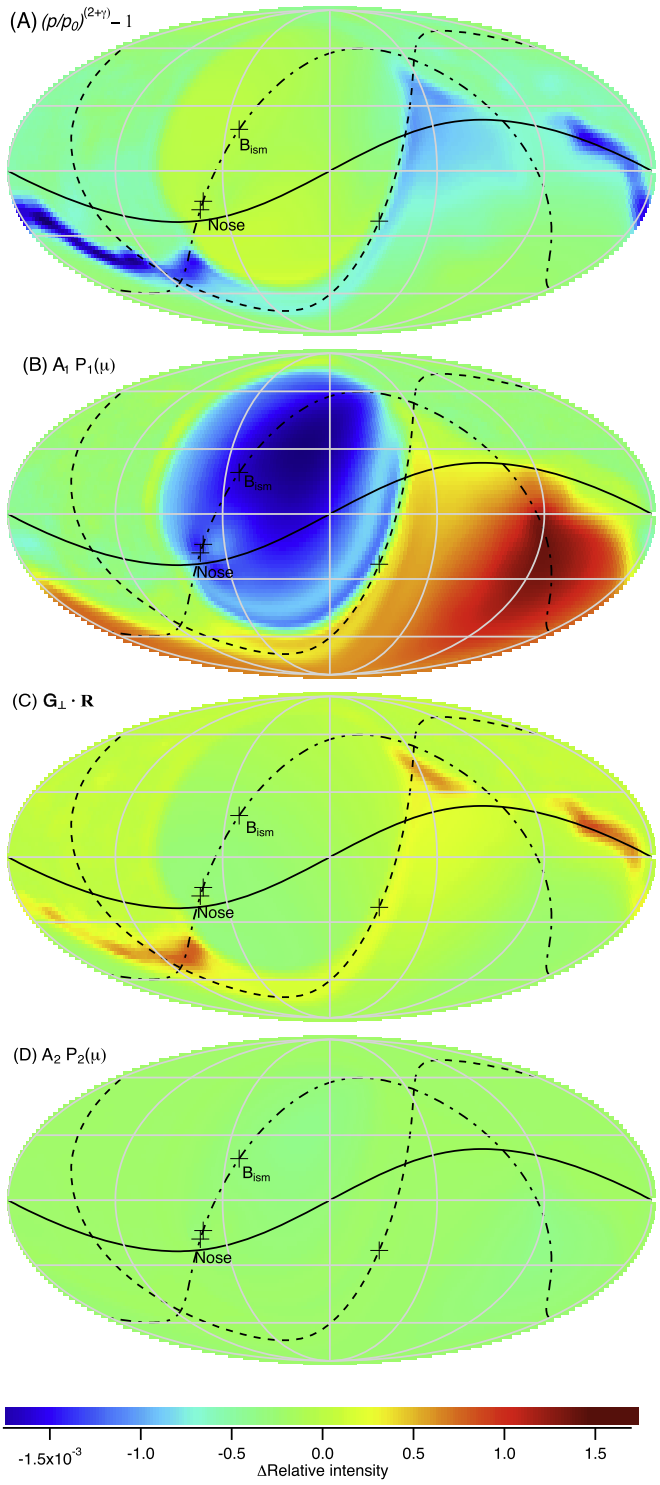

Figure 4. Mechanisms contributing to the CR anisotropy expected at Earth in the model calculation. From top to bottom: (A) Compton–Getting plus heliospheric acceleration effect $(p/p_0)^{-(2+\gamma)} - 1$, (B) pitch-angle dipole $A_1P_1(\mu)$, (C) drift and density gradient $\boldsymbol{G}_\perp \cdot \boldsymbol{R}$, and (D) pitch-angle quadrupole $A_2P_2(\mu)$. All of these contributions are have been distorted by the heliosphere. All of the maps are shown in the same celestial coordinate system as in Figure 1.

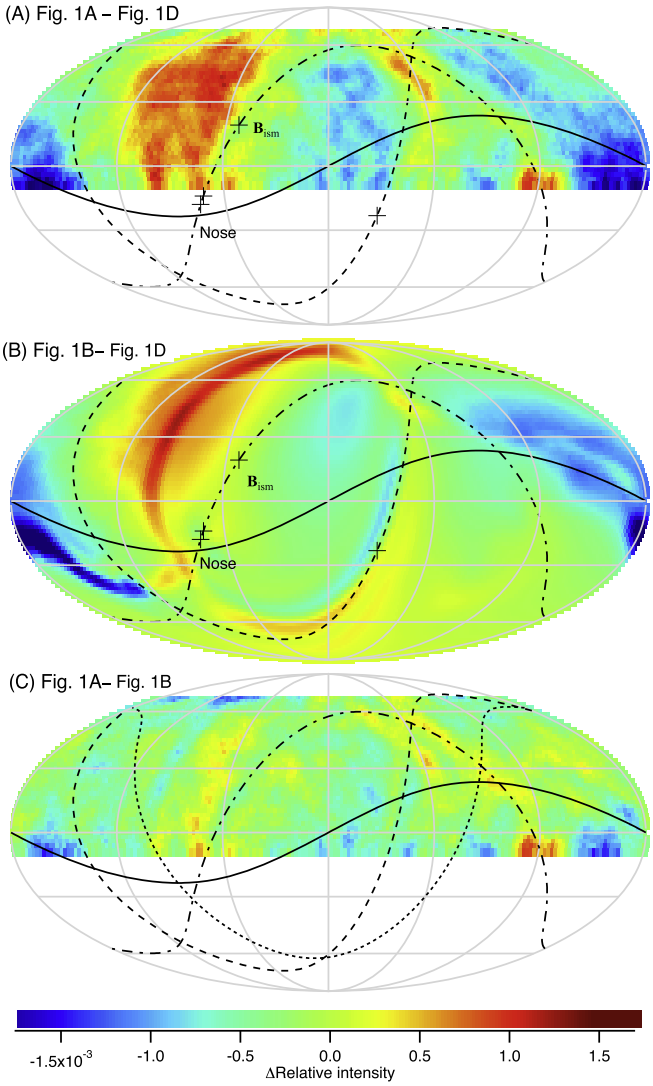

Figure 5. Amount of heliospheric distortion in the Tibet ASγ measurements (A) Figures 1(A)–(D) and in our model calculation (B) Figures 1(B)–(D). Residue CR anisotropy after subtraction of the model calculation from Tibet ASγ measurements (C) Figures 1(A)–(B), showing only small-scale anisotropy left out of the heliospheric distortion model calculation. All of the maps are shown in the same celestial coordinate system as in Figure 1.

Table 1
Parameters in the LISM CR Distribution Function Derived from the Least χ^2 Fit to Tibet ASγ Measurements of Relative Intensity at 4 TeV

Parameter Name	Value
Amplitude of pitch-angle dipole	$A_1 = (0.165 \pm 0.002)\%$
Amplitude of pitch-angle quadrupole	$A_2 = (0.015 \pm 0.002)\%$
CR density gradient	$\lvert\boldsymbol{G}_\perp\rvert = (0.021 \pm 0.001)\%/R_g$
Normalization	$f_0 = 1 + (0.024 \pm 0.001)\%$

Note. The gyroradius R_g of these particles in a 3.5 μG LISMF is 254 au.

arrival directions within 5° of each pixel. This averaging makes the calculated anisotropy map in Figure 1(B) appear smoother. The part of the sky not covered by the Tibet ASγ experiment is lightly shaded. The major features in the un-shaded region match the Tibet ASγ observations quite well. Good fits can also be deduced from the residue map (Figure 1(E)), which only exhibit small-scale anisotropies not included in our model mapping. It can be seen that the $B - V$ plane and the plane that is perpendicular to the LISMF play special roles in defining the anisotropy boundaries seen in the maps. MHD plasma/kinetic neutral atom simulations of the SW–LISM interactions demonstrate that the deflection of neutral

hydrogen atoms from their original direction in the unperturbed LISM observed in the heliosphere by *SOHO* occurs predominantly in the $B-V$ plane (Pogorelov et al. 2009). Thus, the results explain why some features of CR anisotropy are aligned with the HDP. The match of anisotropy features signifies the importance of the heliosphere. Our model runs using different LISMF and ion density parameters all show these anisotropy feature, but the heliosphere model shown in Figures 2 and 3 gives the least χ^2 fit and the best match of feature locations compared with the observations. The results confirm the predictive power of our CR anisotropy mapping model as well as the reliability of model of our heliosphere model and its effects on the surrounding LISM. To fit the CR anisotropy observations, we find that the heliotail should extend beyond 10,000 au downwind; otherwise, more artifacts that do not agree with the measurements would show up in our calculation.

In Figure 4, we separate the calculated anisotropy into a composition of effects associated with changes of particle momentum, guiding center, and pitch angle. The pitch-angle variation is further broken into a dipole and a quadruple to search for possible mirroring of CRs by inhomogeneities in the LISMF. In Figure 5, we show residues of measured anisotropy after it is subtracted by our model calculation. These data demonstrate the quality of our model and its capability to offer detail understanding about the cause of observed anisotropy.

The measurements of relative intensity and its statistical error from the Tibet ASγ experiment are fitted to our model calculation result using the standard least-weighted χ^2 method. The reduced χ^2, or $\chi^2/(M-5)$, of the fit is 4.5, whereas it is supposed to be near 1 for an ideal fit. This is due to the underestimate of error bars of the measured relative intensity for each pixel $\sigma(\boldsymbol{p}_{om})$ used in the calculation of χ^2. The measurements of CR relative intensity suffer a systematic uncertainty due to its poor determination of the exact CR intensity variation in decl. Our heliosphere model has additional uncertainties because the LISMF direction and magnitude, as well as the densities of ions and neutral hydrogen atoms in the unperturbed LISM, are known only indirectly. Both of these uncertainties are hard to quantify. If the underlying error bars used in our calculation of χ^2 are twice the counting statistical errors in the measured CR data, the reduced χ^2 will become close to 1. The error bars of the obtained fitting parameters in Table 1 should also increase by a factor of ~2. The coefficient of determination or goodness of fit,

$$R^2 = 1 - \frac{\sum_{m=1}^{M}[I(\boldsymbol{p}_{om}) - f(\boldsymbol{x}_m, \boldsymbol{p}_m)]^2}{\sum_{m=1}^{M}[I(\boldsymbol{p}_{om}) - \langle I\rangle]^2} = 0.90, \qquad (3)$$

where $\langle I\rangle = 1$. The $R^2 = 0.90$ value indicates very good model predictability, even though we have only a few model parameters.

3.2. Properties of Large-scale CR Anisotropy and Transport in the LISM

The derived LISM CR distribution function yields a CR anisotropy map expected in the pristine LISM (Figure 1(D)). As the contribution of the pitch-angle dipole with amplitude A_1 exceeds the other contributions (see Table 1), the large-scale CR anisotropy in the LISM is essentially a dipole antiparallel to the LISMF. Moreover, the pitch-angle dipole amplitude is even larger than the amplitude of the total observed anisotropy because the heliospheric Compton–Getting effect plus particle acceleration by heliospheric electric field (Figure 4(A)) and drift anisotropies (Figure 4(C)) act to partially cancel the pitch-angle dipole anisotropy (Figure 4(B)).

The amplitude of $A_1 = 0.165\%$ corresponds to a CR flow with flux $F_{||} = 3A_1 cf = 4.95 \times 10^{-3} cf$ along the LISMF into the northern Galactic halo (c is the speed of light). The Sun and its surrounding Local Bubble is part of the tube-like chimney (Local Chimney) that extends through the local region of the spiral disk into the Galactic halo (Welsh et al. 1999; Lallement et al. 2003). The Local Chimney acts as a vent for the hot gas produced by supernova. Although the Local Chimney extends into both the northern and southern halo, the fact that TeV CR flow directs northward along the magnetic field lets us conclude that the Sun is located in the north part of the Local Chimney. This CR flow is strong, equivalent to a bulk motion of $4.95 \times 10^{-3} c = \sim 1500\,\mathrm{km\,s^{-1}}$ speed. Given the dominant energy density of CRs, this flow probably is responsible for opening up the Local Chimney. However, it cannot be a result of convection of the ISM plasma out of the Galactic disk; otherwise, the speed of $\sim 1500\,\mathrm{km\,s^{-1}}$ would show up in the measurement of neutral atoms by *Ulysses* and *IBEX*. It is most likely due to the diffusion process of CRs. Assuming that the parallel diffusion coefficient, $\kappa_{||}$, of 4 TeV CR protons exceeds $10^{29}\ \mathrm{cm^2\,s^{-1}}$, we arrive at the density gradient of $|\nabla_{||} \ln f| < 2.23 \times 10^{-8}\,\mathrm{au^{-1}}$, or $1.40 \times 10^{-3}\,\mathrm{lt\text{-}yr^{-1}}$ pointing southward opposite to the magnetic field. If such magnitude of parallel density gradient persists into the halo and the inclination of the magnetic field to the Galactic plane remains constant, we predict that the half-thickness of the CR disk in the vicinity of the Sun is greater than 440 lt-yr. The CR disk will be proportionally thicker if the diffusion coefficient is larger. The CR density gradient perpendicular to the LISMF has the magnitude of $|G_\perp| = |\nabla_\perp \ln f| = 0.021\%/R_g$, which is equal to $8.2 \times 10^{-7}\,\mathrm{au^{-1}}$, or $5.2 \times 10^{-2}\,\mathrm{lt\text{-}yr^{-1}}$. It is much larger than that in the parallel direction. The density gradient of this magnitude means that the CR density changes e (=2.718) times every 19 lt-yr, which implies large CR density variations in the solar vicinity. The direction of perpendicular density gradient is shown in Figure 1(D). It approximately points toward Vela located in the Local Bubble. The direction is about 25° off the Galactic plane northward. As the parallel component of density gradient is too small to be identified due to the dominance of parallel diffusion, the direction of the perpendicular component of density gradient does not rule out the possibility that the source is in the Galactic disk. Although the density gradient is predominantly in the direction perpendicular to the LISMF, the maximum diffusion flux it generates is $F_\perp < 7.0 \times 10^{-5} cf$. This is because the diffusion coefficient perpendicular to the local magnetic field, $\kappa_{\perp\mathrm{LISM}}$, must be less than the Bohm diffusion limit of $cR_g/3$, or $3.8 \times 10^{25}\ \mathrm{cm^2\,s^{-1}}$. Such a perpendicular diffusion flow is still much weaker than the parallel diffusion flow.

The results presented above imply that parallel diffusion dominates in the CR transport in the LISM, whereas the density gradient is primarily in the perpendicular direction. Such a situation can only occur if CR diffusion is highly anisotropic, the mean free path parallel to the magnetic field being much greater than that in the perpendicular direction. CRs propagate mostly along magnetic field lines connected to their sources. To spread CRs over the entire Galaxy, including the halo, a random walk of magnetic field lines is necessary. On the

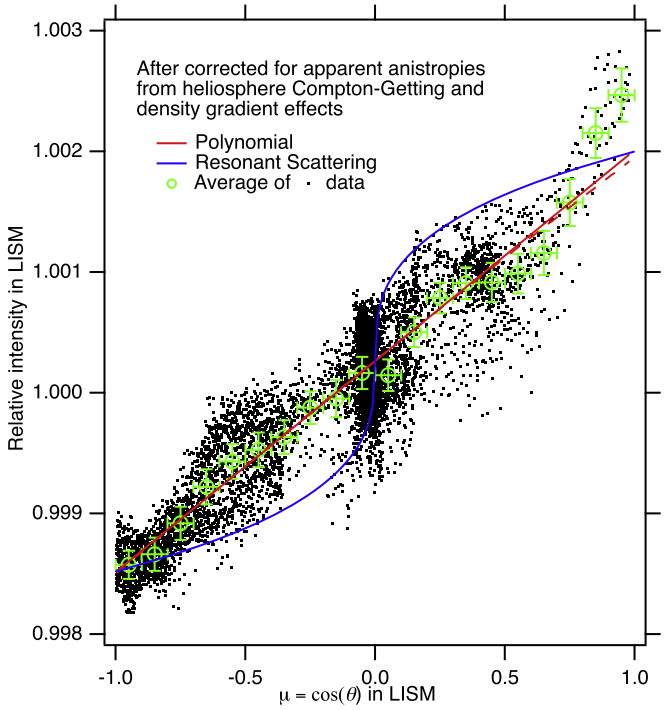

Figure 6. Distribution of CR relative density as a function of the cosine of particle pitch angle in the LISM. The green symbols with error bar are the averages binned in equal pitch-angle cosine intervals. The distribution has been corrected the measurements for the gyrophase-dependent anisotropies from the effects of Compton–Getting, particle acceleration and drift in the heliosphere so that the pitch-angle distribution becomes nearly gyrotropic. The red solid line is a polynomial fit, but it is essentially the same as a straight-line fit (red dashed line). The blue curve is the pitch-angle distribution expected from resonant particle scattering by Alfvénic turbulence with a Kolmogorov spectrum.

Galactic scale, CRs behave as if they can effectively propagate across the average ISMF.

3.3. Properties of Pitch-angle Scattering by the LISM Turbulence

Equation (1) states that any measured anisotropy is a combined variation of the particle distribution function as a function of momentum, position, and pitch angle. The Compton–Getting and heliospheric acceleration effects show up as p deviates from the observed momentum p_o. Drift anisotropy is represented by the scalar product $\boldsymbol{G}_\perp \cdot \boldsymbol{R}$. We can obtain the genuine pitch-angle distribution of CRs in the LISM by subtracting the effects of Compton–Getting, acceleration, and drift anisotropies caused by the heliosphere from the measurements, or Figure 1(A)—(Figures 4(A) + (C)). Figure 6 shows its dependence on the pitch-angle cosine μ of CRs originally in the LISM. First of all, it appears to be independent of the particle gyrophase, which is another possible angular variable contained in each data point. This means that the CR distribution in the LISM plasma frame is gyrotropic. This is not surprising, because TeV CRs are strongly magnetized when particle gyroradii are small compared with the correlation length of turbulence. The quality of gyrotropy derived from the data also imposes constraints on our heliosphere model. Actually, it was one of the criteria for choosing specific LISMF and plasma conditions in our heliospheric simulation.

Surprisingly, the LISM CR pitch-angle distribution is nearly proportional to μ. In the quasilinear theory of wave–particle interaction (Schlickeiser 1989), particle pitch-angle distribution can be expressed as

$$f(\mu) - f(0) = -\frac{\partial f}{\partial p}\int_0^\mu \frac{D_{\mu p}(\nu)}{D_{\mu\mu}(\nu)}d\nu - \frac{c}{2}\nabla_{\|} f \int_0^\mu \frac{1-\nu^2}{D_{\mu\mu}(\nu)}d\nu, \quad (4)$$

where $D_{\mu\mu}$ is the pitch-angle diffusion coefficient, and $D_{\mu p}$ is the cross diffusion coefficient of μ and momentum p. The first term stems from the spectral slope of the momentum distribution. If the diffusion is driven by an Alfvén wave train propagating at the Alfvén speed V_A along the magnetic field, $D_{\mu p}/D_{\mu\mu} = V_A/c$. Integration of this term automatically yields a pitch-angle distribution proportional to μ. Effectively, this term can be understood as the Compton–Getting effect in the reference frame comoving with the wave. In an ensemble of counterpropagating plasma waves, $D_{\mu p}/D_{\mu\mu}$ is reduced to $H_c V_A/c$, where H_c is the normalized cross helicity, which specifies the percentage difference of the wave power between forward and backward propagating waves. However, the Alfvén speed is about 30 km s^{-1} in the LISM, so even if all waves propagate in one direction with an ideal cross helicity equal to -1, it is still difficult to account for the observed pitch-angle anisotropy of a much larger amplitude, which would require an Alfvén speed of about 100 km s^{-1}.

A more probable explanation to the observed anisotropy is the combined action of pitch-angle diffusion and CR density gradient from the second term of Equation (4), which creates a spatial diffusion flow parallel to the magnetic field. The linear character of the pitch-angle distribution shown in Figure 6 indicates that the strength of pitch-angle scattering of CRs in the LISM is nearly isotropic (red line), or $D_{\mu\mu} \propto (1-\mu^2)$. Resonant scattering of CRs by static Alfvénic turbulence with a Kolmogorov spectrum (blue line) would produce a $f(\mu) - f(0) \propto \mu^{1/3}$, and therefore is inconsistent with the observations. The isotropic character of pitch-angle scattering is likely to impose tight constraints on the properties of LISM turbulence. It is possible that the LISM turbulence is highly compressive or dynamic (Yan & Lazarian 2008), but further study is necessary to understand this issue.

The amplitude A_2 of pitch-angle quadrupole is more than 10 times less than the dipole amplitude A_1. Its contribution to the observed anisotropy is hardly visible in Figure 4(D). Small second-order anisotropy observed in the LISM indicates that there is little mirroring of the CR flow. This suggests that the LISMF strength is rather uniform on scales of the particle mean free path, which is about a few light years.

3.4. Angular Power Spectrum of CR Anisotropy in the LISM

The 2D map of relative intensity can be expanded in terms of a linear combination of spherical harmonics,

$$f = \sum_{\ell=0}^{\ell_{\max}} \sum_{m=-\ell}^{\ell} a_{\ell m} Y_{\ell m}. \quad (5)$$

The angular spectral power of a multipole of order ℓ is associated with the presence of structures in the sky on angular

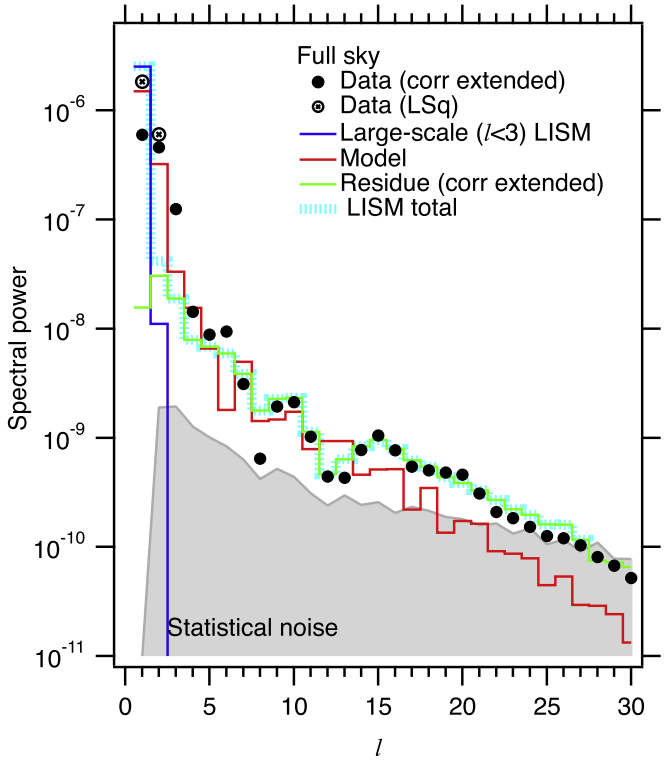

Figure 7. Angular power spectrum of CR anisotropy. Tibet ASγ measurements are shown with black symbols. The red line is from our model of heliospheric distortion. The green line shows the residual spectrum of measurements after subtraction of the model result. The blue line is derived from the inferred large-scale ($\ell < 3$) original anisotropy in the LISM. The true original LISM anisotropy spectrum is represented with the thick teal line.

scales of about $180^\circ/\ell$. It can be calculated as the averaged amplitude square in harmonics of order ℓ (Abbasi et al. 2011), or $\sum_{m=-\ell}^{\ell}|a_{\ell m}|^2/(2\ell+1)$. In the case of complete and uniform sky coverage, a straightforward Fourier decomposition (e.g., Driscoll & Healy 1994) of the relative intensity maps would yield an unbiased estimate for the power spectrum. Unfortunately, this can be done only for our model simulations, but not for the measurements. Due to the limited sky exposure of CR air shower experiments on the ground, we just make a direct assessment of the so-called pseudo-power spectrum, which is calculated by assuming that the CR intensity variation is 0 in the unexposed part of the sky. To assess the power spectrum of anisotropy on the full sky, we have to make some assumptions. The IceCube team (Abbasi et al. 2011; Abeysekara et al. 2019) use the publicly available PolSpice software (Challinor et al. 2018) developed originally to analyze the cosmic microwave background data from, e.g., NASA *Wilkinson Microwave Anisotropy Probe* mission. The software corrects for the two-point correlation function with that of exposure mask function (Ansari & Magneville 2010). However, other assumptions can be made, and the result of spectral power estimation can be different by a factor up to the ratio of the full sky to the exposed area coverage, which is particularly sensitive for low-order harmonics.

In Figure 7, the spectra of the calculated (red line) and inferred large-scale ($\ell < 3$) LISM anisotropies (blue line) are derived from the full-sky maps shown in Figures 1(B) and (D), respectively. Because the LISM CR distribution function in our model is truncated beyond the quadrupole, the spectral power of calculated anisotropy above $\ell = 2$ (red line) is generated entirely by the heliosphere. The Tibet ASγ measurements cover only a partial sky, so we use two different assumptions for the unexposed part of the sky when assessing the spectral power. The result obtained with PolSpice software is shown with the black dots labeled "corr extended" in Figure 7. We also calculated the spectral power of the measured anisotropy for $\ell = 1$ and $\ell = 2$ using a least square fit technique (see black cross-circle symbols labeled "LSq"). The spectral power is somewhat sensitive to the assumptions used to treat the unexposed part of the sky, particularly at low ℓ. The spectral power of the residue (Figure 5(C)), i.e., the difference between the measurement and model, is shown in green color. The residue consists of anisotropies not considered in our model calculations.

Comparing the spectra of calculated anisotropy (red) and Tibet ASγ measurement (black), we found that the heliosphere-induced anisotropy can account for the majority of the spectral power below $\ell = 13$. The residue spectrum (green) has much less power in $\ell = 1$ and $\ell = 2$ compared with the measurement, which indicates that our model has taken care of the large-scale anisotropy adequately. For $\ell > 13$, the spectral power in the residue exceeds the heliosphere-induced anisotropy, indicating that these harmonics are small-scale anisotropies originated in the LISM. The sum of the large- (blue) and small-scale (green) LISM anisotropies (the thick teal line) gives us the true power spectrum of CR anisotropy in the LISM. The dipole contribution ($\ell = 1$) dominates the LISM anisotropy spectrum by two orders of magnitude over other multipoles, including $\ell = 2$. We therefore conclude that the pattern of CR anisotropy in the LISM is almost a pure dipole consistent with diffusion of CRs parallel to the LISMF. The effect of turbulent fluctuations and magnetic mirroring are much smaller than the dipolar anisotropy from CR diffusion. Thus, if it were not for the dipole contribution and heliosphere distortion effects, the CR intensity in the LISM would be rather smooth. Because the heliosphere can already account for the most of the observed spectral power in the middle scales between $\ell = 2$ and $\ell = 12$, the required fluctuation level and spatial scale sizes of the ISM turbulence may have to be significantly modified from previous estimates (Giacinti & Sigl 2012; Ahlers & Mertsch 2015).

4. Discussion: Is Vela a Special Source of TeV CRs?

Given the large CR density gradient of 5.2×10^{-2} lt-yr^{-1} derived from our analysis, we conclude that one or a few local recent supernova sources are producing a significant fraction of observed CRs. Otherwise, the global inhomogeneity of CR sources would most likely make the density gradient of these CRs persist over thousands of light years, which would create very large variations in the diffuse gamma-ray emission over the Galaxy disk; this is not observed. In Figure 8, we project the LISMF direction and CR density gradient onto the Galactic plane with distributions of ISM and OB stars shown in the background. The density gradient points toward the Local Bubble. It suggests that the Local Bubble is a significant source of CRs we see at Earth. Based on measurements of ^{22}Ne/^{20}Ne ratio in GeV CRs, Binns et al. (2005) estimated that a significant fraction of CRs comes from material left behind by Wolf–Rayet stars in the superbubble. To accelerate particles to >TeV energies, we need strong shocks such as those driven by supernovae. Vela is in the Local Bubble, and it is surrounded

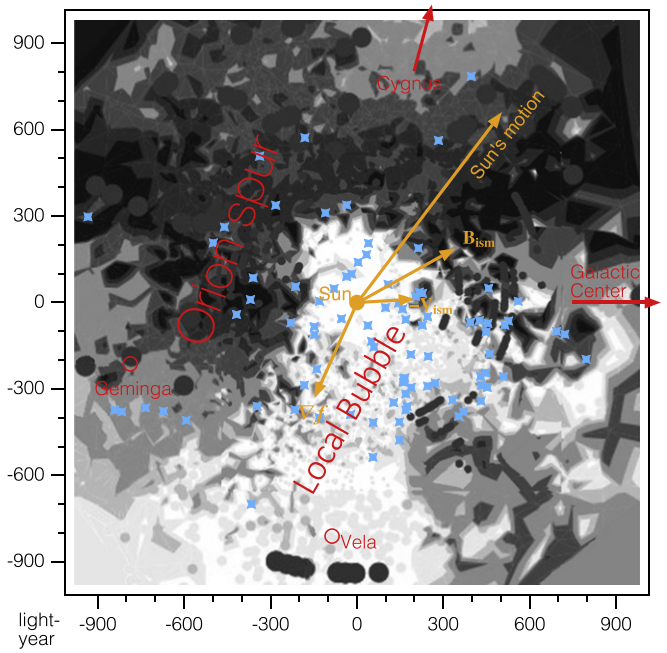

Figure 8. Directions of LISMF ($\boldsymbol{B}_{\rm ism}$), CR density gradient (∇f), and inflow of LISM relative to the Sun ($-\boldsymbol{V}_{\rm ism}$) projected on the Galactic plane with a picture of the LISM environment. Cumulative extinction of interstellar dust is used to approximate the ISM density on a gray scale where the darker color means denser ISM (adapted from Frisch & Dwarkadas 2017). The blue symbols indicate the locations of bright OB stars in the region.

by materials from Wolf–Rayet stars. Thus, it is a natural tendency to consider Vela as a local source of CRs.

Is Vela a possible significant contributor to the observed anisotropy? It is one of the possibilities derived through analyzing the dipole anisotropy phase angle of 100–300 TeV CRs (Ahlers 2016). Let us treat CR transport from a nearby source as a diffusion process without energy loss or nuclear reactions. The solution to the anisotropic diffusion equation with an initial injection of N_1 particles at a point source that exploded time t ago at parallel distance $\boldsymbol{x}_{||}$ and perpendicular distance $\boldsymbol{x}_{\perp}$ can be written as

$$f_1 = \frac{N_1}{\sqrt{64\pi^3\kappa_{||}\kappa_{\perp}^2 t^3}} \exp\left(-\frac{\boldsymbol{x}_{||}^2}{4\kappa_{||}t} - \frac{\boldsymbol{x}_{\perp}^2}{4\kappa_{\perp}t}\right). \quad (6)$$

The formula is roughly the same for a curved magnetic field, with the exception that distances should be given in a curvilinear coordinates system. In the diffusion approximation, the anisotropy in the plasma frame of CRs from single point source can be derived from the diffusion flow, so the anisotropy amplitude of CRs from this source $\boldsymbol{A}_1 = -3\boldsymbol{\kappa}\cdot\nabla \ln f_1/c = 3(\boldsymbol{x}_{||}+\boldsymbol{x}_{\perp})/2ct$, where the density gradient is $\nabla \ln f_1 = -(\boldsymbol{x}_{||}/\kappa_{||} + \boldsymbol{x}_{\perp}/\kappa_{\perp})/2t$. If all other past supernovae are responsible for the isotropic part of the total CR density f, the resulting anisotropy and density gradient are both reduced by the factor of f_1/f.

By our determination of CR anisotropy and gradient, we conclude that $|\boldsymbol{x}_{||}| \gg |\boldsymbol{x}_{\perp}|$ and $|\boldsymbol{x}_{||}|/\kappa_{||} \ll |\boldsymbol{x}_{\perp}|/\kappa_{\perp}$. The maximum possible anisotropy due to the Vela supernova, which occurred 11 kyr ago at a distance of 815 lt-yr away from the solar system, is 11%, provided that all CRs that we measure come from Vela. The observed anisotropy amplitude and density gradient imply that only $f_1/f = 1.5\%$ of them are from Vela, while $|\boldsymbol{x}_{\perp}| = 1.5\times10^5\kappa_{\perp}/c = 5.0\times10^4\lambda_{\perp}$, where $\lambda_{\perp}$ is the particle mean free path perpendicular to ISMF.

The ratio of f_1/f can be used to estimate the distance to the recent local source and to calculate the diffusion coefficient perpendicular to the LISMF. We can use a leaky box model to estimate the intensity of CRs produced by all sources in the Galaxy. Assume that the density of the rest CRs is uniform and isotropic inside the Galactic disk (100 lt-yr in radius and 880 lt-yr in thickness) and that they come from identical supernovae exploding randomly every 30 yr during the last 10 Myr of CR lifetime. The CR density f is equal to the total number of CRs released during the lifetime divided by the volume of the Galactic disk. Using the ratio of $f_1/f = 1.5\%$, we estimate that the perpendicular distance to Vela should be ~122 lt-yr and a $\kappa_{\perp}/\kappa_{||}$ ratio of about 8.9×10^{-4} is needed. The results are obtained with a $\kappa_{||} = 10^{29}\,{\rm cm^2\,s^{-1}}$, but they are insensitive to the exact number of $\kappa_{||}$ in this order of magnitude. A straight extrapolation of the LISMF all the way from the Sun to Vela yields a much larger (750 lt-yr) perpendicular distance. If Vela is indeed the source of these CRs, the LISMF lines must somehow bend toward it by ~50°. Alternatively, if a supernova exploded in the Local Bubble 815 lt-yr from us and slightly longer time of 30 kyr ago, the required perpendicular distance can be increased to ~323 lt-yr. The corresponding diffusion coefficient ratio increases to 1.4×10^{-3}. The estimated perpendicular diffusion coefficient is slightly larger than the Bohm diffusion limit in a 3.5 μG field, so it must include the effect of the large-scale random walk of magnetic field lines. A higher fraction (~4.0%) of CRs should come from the source. In this case, less bending of magnetic field lines is necessary. The latter scenario is perhaps more likely, but we cannot rule out Vela completely. The distance and age of the contributing supernova need to be constrained together. Vela Jr., which exploded 700 lt-yr away and 1 kyr ago, is too young to be a possible source because it requires an almost direct connection by magnetic field lines. A supernova of similar distance but much older than 60 kyr will also have difficulty satisfying the observation. Supernova remnants in the low-density Local Bubble should live longer than 60 kyr so we should be able to see any younger supernova in the Local Bubble. In fact, Vela is the only one satisfying the age requirement. Thus, we suggest that Vela might have made a significant contribution to the observed TeV CR anisotropy. If this is true, the intensity of CRs at Earth will keep rising in the future as estimation using Equation (6) yields that the peak time of CR intensity from Vela should occur at more than hundreds kyr. We acknowledge that complicated magnetic field geometry between the solar system and Vela in the Local Bubble might invalidate this suggestion by our simple estimate, particularly for a situation when the Sun is located in the boundary of Loop 1 superbubble (Frisch 2014; Xu & Han 2019). More detailed modeling is needed. The proposed scenario can also be further tested by measurements of CR energy spectrum and composition, as well as other remote-sensing observations of the ISM gas as the Local Bubble consists of multiple explosions of OB stars.

5. Conclusion

Based on a state-of-art MHD heliosphere model, we have corrected particle propagation effects with the help of the Liouville theorem. We found that the original anisotropy of TeV CRs in the LISM is nearly a pure dipole oriented antiparallel to the LISMF. It is consistent with a diffusion flow

of CRs escaping the Galactic disk into the northern Galactic halo along the magnetic field lines. The pitch-distribution of CRs in the LISM is linearly proportional to pitch-angle cosine, indicating that particle scattering by ISM turbulence is nearly isotropic. Higher-order multipole anisotropies in the LISM are much weaker than the dipole. The electromagnetic fields of the heliosphere can distort the LISM CR dipole anisotropy and generate high-order multipole anisotropies that make observations at Earth look complicated. On the medium scales, the observed anisotropies can almost entirely be accounted for by the heliospheric effect. Only on small scales, the observed anisotropies may come from those originally in the LISM, but their amplitudes are rather small, suggesting weak influence by ISM turbulence.

We also have determined the density gradient of TeV CRs. The gradient is perpendicular to the LISMF and points approximately toward the Vela supernova remnant behind the Local Bubble. It confirms that the Local Bubble could be a local source group of CRs that we observe at Earth. Further analysis using diffusive CR transport suggests that Vela might be a discrete source of these CRs.

This work was supported by NASA grants NNX15AN72G, NNX15AN72G, 80NSSC18K0644, and 80NSSC18K1649NS; NSF awards OAC-1811176 and XSEDE MCA07S033; NNSF of China grant 11851303; and Deutsche Forschungsgemeinschaft grant Schl 201/34-1.

ORCID iDs

Ming Zhang https://orcid.org/0000-0003-3529-8743
N. V. Pogorelov https://orcid.org/0000-0002-6409-2392
R. Schlickeiser https://orcid.org/0000-0003-3171-5079

References

Abbasi, R., Abdou, Y., Abu-Zayyad, T., et al. 2011, ApJ, 740, 16
Abeysekara, A. U., Alfaro, R., Alvarez, C., et al. 2019, ApJ, 871, 96
Ahlers, M. 2016, PhRvL, 117, 151103
Ahlers, M., & Mertsch, P. 2015, ApJL, 815, L2
Amenomori, M., Ayabe, S., Bi, X. J., et al. 2006, Sci, 314, 439
Amenomori, M. & The Tibet ASγ Collaboration 2010, ASTRA, 6, 49
Ansari, R., & Magneville, C. 2010, MNRAS, 405, 1421
Binns, W. R., Wiedenbeck, M. E., Arnould, M., et al. 2005, ApJ, 634, 351
Bradt, H., & Olbert, S. 2008, Astrophysical Processes (Cambridge: Cambridge Univ. Press)
Challinor, A., Chon, G., Colombi, S., et al. 2018, Spatially Inhomogeneous Correlation Estimator for Temperature and Polarisation, http://www2.iap.fr/users/hivon/software/PolSpice/
Compton, A., & Getting, I. 1935, PhRv, 47, 817
Desiati, P., & Lazarian, A. 2013, ApJ, 762, 44
Driscoll, J., & Heally, D. 1994, AdApM, 15, 202
Frisch, P. 2014, JPhCS, 531, 012005
Frisch, P. C., & Dwarkadas, V. V. 2017, in Handbook of Supernovae, ed. P. Alsabti & A. W. Murdin (Cham: Springer International Publishing), 2253
Giacinti, G., & Sigl, G. 2012, PhRvL, 109, 071101
Lallement, R., Welsh, B. Y., Vergely, J. L., Crifo, F., & Sfeir, D. 2003, A&A, 411, 447
McComas, D. J., Bzowski, M., Frisch, P., et al. 2010, JGRA, 115, A09113
O'C Drury, L. 2013, Proc. ICRC, (Rio de Janeiro, Brazil), 2, 835
Pogorelov, N., Borovikov, S., Heerikhuisen, J., & Zhang, M. 2015, ApJL, 812, L6
Pogorelov, N., Fichtner, H., Czechowski, A., et al. 2017, SSRv, 212, 193
Pogorelov, N. V., Heerikhusen, J., Zank, G. P., & Borovikov, S. 2009, SSRv, 143, 31
Schlickeiser, R. 1989, ApJ, 336, 243
Schwadron, N., Adams, F. C., Christian, E. R., et al. 2014, Sci, 343, 988
Taylor, J. 1997, An Introduction to Error Analysis (2nd ed.; Sausalito, CA: Univ. Science Books)
Welsh, B., Sfeir, D., Sirk, M., & Lallement, R. 1999, A&A, 352, 308
Xu, J., & Han, J. L. 2019, MNRAS, 486, 4275
Yan, H., & Lazarian, A. 2008, ApJ, 673, 942
Zhang, M., Zuo, P., & Pogorelov, N. 2014, ApJ, 790, 5
Zirnstein, E., Heerikhuisen, J., Funsten, H. O., et al. 2016, ApJL, 818, L18